Proceeding Paper.

Preparation, Properties, and Characterization of ZnS nanoparticles

Amani H. Ali,* , H. A. Hashem[1] and A. Elfalaky[1]

hahashem@gmail.com (H.A.); a.elfalaky@gmail.com (A.E)

* Correspondence: amany.hamdy84@yahoo.com

† Presented at 6th International Electronic Conference on Atmospheric Sciences, 01–15 December 2022; Available online: https://ecas2022.sciforum.net/.

Abstract: This paper studied, the structural, microstructural, thermal, electrical, and dielectric properties of the synthesized ZnS nanoparticles using co-precipitation technique. The precipitate was characterized using X-ray diffraction (XRD). Characterization was confirmed via formation of a single-phase cubic nanocrystal line structure. Crystalline size was obtained with different three models. Information regarding thermal transition such as melting, oxidation, and crystallization was revealed using Differential scanning calorimetry and thermogravimetry (DTG/TG). Transmission electron microscopy (TEM) images were performed to explore the stability, morphology, and other properties of ZnS nanoparticles. For the importance of the crystallite size of the prepared ZnS, different techniques were utilized to estimate the crystallite size, and the calculations confirmed the formation of ZnS in nanocrystal form. The electrical properties of the synthesized nanocrystals were measured at different temperatures 293 -373 K over a wide range of frequencies from about 50 Hz up to 5 MHz. Regarding the frequency dependence of both the AC conductivity. The Activation energy (E_a) was found to decrease with increasing frequency.

Keywords: ZnS; Activation energy; AC conductivity; dielectric constant; electric modulus

1. Introduction

ZnS nanomaterials, including II-VI binary compounds, got tremendous attention because of their intriguing properties arisen from size quantization and extremely high surface to volume ratio of these materials, which offer major advantages over their bulk materials. Nano-materials have sublime physical and chemical properties, which are more efficient than bulk materials. These unique properties occur when there is a change in some features like variation of size and band gap energy.

Zinc sulfide nanomaterial is non-toxic material, which is chemically more stable than other semiconductors and it is characterized with a wide band-gap energy of ~3.7 eV. Because of these properties are at the origin of diverse promising applications such as ultraviolet light sensors , efficient UV light emitting diodes , optoelectronic devices and electroluminescent applications . The photoemission wavelengths, the band gap and the lattice parameter are strongly dependent on the grain size. There are many techniques used to prepare ZnS in nanomaterial form, such as microwave irradiation technique [1, 2], sol - gel, electrochemical deposition, [3] sonochemical, hydrothermal technique and low-temperature microemulsion [4].

In this work, ZnS nanoparticles were prepared using a chemical co-precipitation method. Structural and morphological properties have been investigated using X-ray diffraction. The electrical studies have been carried out within a frequency range of 50Hz to 5MHz at different temperatures.

2. Materials and Methods

The following materials were needed for preparation of the ZnS nano-materials: $ZnCl_2$, Sodium Sulfide non hydrate $Na_2S.9H_2O$ (assay 99.5%), Sodium hydroxide NaOH from Alpha Chemika and Butan $CH_3.(CH_2)_3.OH$ from El-Nasr Pharmaceutical Chemical Company.

ZnS nanoparticles have been synthesized employing co-precipitation technique. Molecular weight of the reactants as $Na_2S.9H_2O$ as 46.51gm were dissolved into 500 ml of distilled water at room temperature under stirring for 30 minutes until an aqueous solution of concentration $ZnCl_2$ as 34.075 gm was dissolved into 500 ml distilled water under continuous stirring for 30 minutes to get an aqueous solution . A substitution reaction will take place according to the following equation:

$$ZnCl_2 + Na_2S.9H_2O + \xrightarrow{\quad NaOH \quad} ZnS + 2NaCl + 9H_2O \tag{1}$$

After adding the first and second solutions to each other, few drops of NaOH (as a catalyst) were added under continuous stirring for 30 minutes. The color of the aqueous medium was converted to whitish color immediately due to formation of ZnS. The stirring was continued further for a specific time in order to facilitate complete nanoparticle precipitation. The value of pH of the solution equals to 12.82. In order to get rid of NaCl the precipitate was washed several times with distilled water and then a whitish powder of ZnS was obtained. The prepared powder pressed under a constant pressure of 1000 pa using a small amount of butane alcohol as a binding material. The sample was pressed in a disk shape of thickness 1.83 mm. The disk coated with silver paste solution for better electrical contacts.

The phase purity and crystal structure of as prepared pure ZnS nanoparticles were carried out by analyzing the X-Ray Diffraction (XRD) patterns using monochromatic Cu-Kα radiation in 2θ range of 10º to 80 º with a X' Pert PRO Diffractometer (XPERT-MPDUG, Philips PW 3040). A JEOL-Transmission Electron Microscopy (TEM) (Model Jeol JEM-1230) was used to record the size of the samples of pure ZnS nanoparticles. The FTIR spectra of the samples were recorded with Shimadzu spectrophotometer in the range of 4000-400 cm^{-1} using KBr pellet technique. The RCL computerized bridge model Hioki 3532 Hitester, used for the measurement of electrical properties sample pellets of uniform thickness were prepared, and silver paste was coated on two extreme surfaces of the pallet to make those surfaces conducting.

3. Results and discussion

3.1. Structural analysis

XRD pattern of the ZnS particles with indexed peaks as (111), (200), (220), (311), (400) and (331) is shown in Error! Reference source not found.,its clear that the pattern represents a polycrystalline material. One can also observe that the peaks are significantly broad. Such results confirm that the particles are of nano-sized crystals according to the (ICDD) reference card No. 04-004-3804 the pronounced peaks correspond to the cubic crystal system [5]. The spacing between the planes of the crystal is d and lattice parameters a, b, c, for (hkl) has been calculated by the following, Eq(2) [6] , which found to be 5.404 Å and the corresponding value was 5.392 Å.

$$\frac{1}{d^2} = \frac{h^2}{a^2} + \frac{k^2}{b^2} + \frac{l^2}{c^2} \tag{2}$$
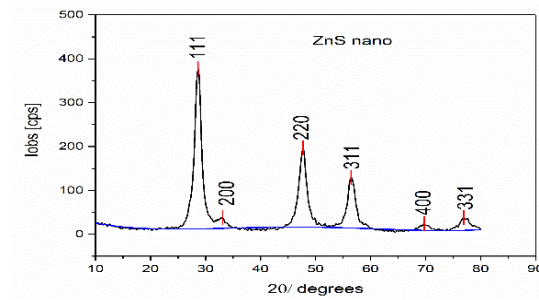
Figure 1. X-Ray patterns of synthesized ZnS nanocrystal
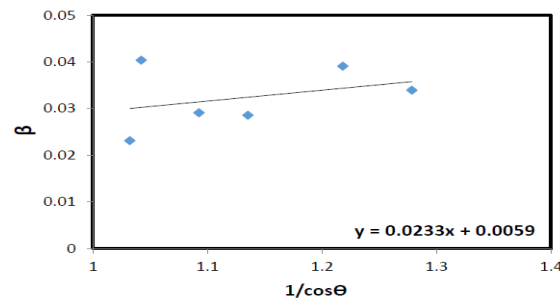
Figure 2. Debye-sherer plot for ZnS.

Two methods were used to investigate the crystalline size of the nanoparticles, the Scherrer method and Williamson–Hall Method (W-H), The average crystalline size of ZnS was calculated to be about 6.3 by Debye– Scherrer's formula $D=0.9\lambda/\beta\cos\theta$ [7, 8], Where D is the crystallite size, λ is the wavelength of X-rays, β is the full-width at half-maxima (FWHM) in radians and θ is the diffraction angle as shown in fig.2 and dislocation density is calculated using $\delta=1/D^2$ [9].
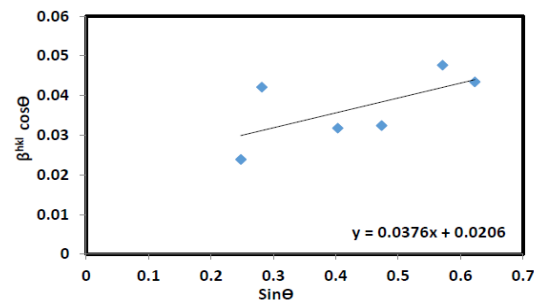
Fig. 3: The W-H plot of ZnS nanoparticles: The uniform deformation model (UDM)
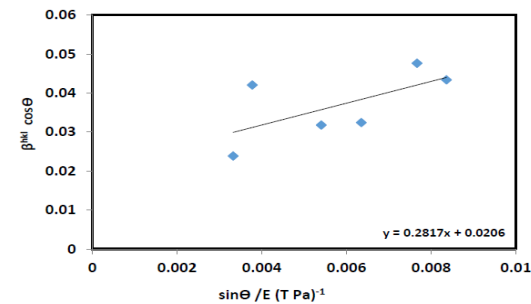
Fig. 4: The W-H plot of ZnS nanoparticles, the uniform deformation strain model (UDSM).
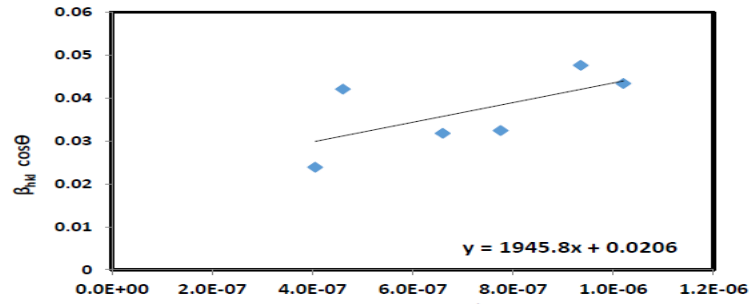
Fig 5: The W-H plot of ZnS nanoparticles: The uniform
deformation energy density model (UDEDM)

W–H [10] method relies on the principle that the approximate formula for size broadening (β) and strain broadening ($\beta\varepsilon$), vary quite differently with respect to the Bragg angle, θ [11]. The strain induced broadening arising from crystal imperfection and distortion can be related as in Eq. (2). The maximum tensile strain alone or maximum compressive strain alone can be calculated from the observed broadening. If both crystallite size and strain contributions present independently of each other, then their combined effects can be determined by convolution. The simplification of W–H is to assume the convolution is a sum of β and βc. using the form of [8].

$$B_{hkl} = B + B_\varepsilon \qquad (2)$$

$$B_{hkl} = \frac{k\lambda}{D\cos\theta} + 4\,\varepsilon\,\tan\theta \qquad (3)$$

By rearranging the above equation, we get

$$B_{hkl}\cos\theta = \frac{k\lambda}{D} + 4\,\varepsilon\,\tan\theta \qquad (4)$$

Eq. (4) represents the uniform deformation model (UDM), where the strain is assumed uniform in all crystallographic directions.The plot in Fig. (3) shows $\beta_{hkl}\cos\theta$ against $\sin\theta$ would give crystallite size that corresponds to the y-intercept and strain due to lattice deformation in the sample that can be calculated from the slope of graph. The graph indicates that ZnS exhibits a positive gradient, which represents the positive strain in the sample.

The uniform deformation strain model (UDSM) and the uniform deformation energy density model (UDEDM) were used where the anisotropic nature of Young's modulus, E of the ZnS and is more realistic. A generalized Hooke's law refers to linear proportionality between the stress and strain as given by $\sigma = E_{hkl}\,.\varepsilon$, where σ is the stress in the surface and E_{hkl} is Young's modulus in the direction perpendicular to the set of crystal lattice planes (hkl). The (W–H) Eq. (4) is then modified by substituting the value of ε [7] and we get Eq. (5)

$$B_{hkl}\cos\theta = \frac{k\lambda}{D} + 4\,\frac{\sigma\sin\theta}{E_{hkl}} \qquad (5)$$

The modulus of elasticity is perpendicular to the crystal lattice planes (hkl). The value of Young's modulus for pure ZnS is 74.5 GPa. [13]. The stress (σ) and crystallite size (D) were calculated from the linear equation shown in figure 4 to represent the model (UDSM). In principle, materials are not always homogenous and isotropic. Agglomerates, defects, dislocations, etc. are subject to imperfections in materials. These facts suggest another model, where the constants of proportionality associated with strain-stress relation are no longer independent. The strain energy density (μ) is considered. According to Hooke's law, the energy density (μ) that is to say, the following relation [12] gives energy per unit volume as function of stain (ε):

$$\mu = \varepsilon 2\, E_{hkl}/2 \qquad (6)$$

The uniform deformation energy density model (UDEDM) can thus be used to estimate the crystallite size (D), strain (ε) and energy density (μ). In this model, the Williamson-Hall equation is written as:

$$\beta_{hkl}\cos\theta = \frac{k\lambda}{D} + 4\sin\theta\,\frac{2\mu}{\sqrt{2/E_{hkl}}} \qquad (7)$$

From the linear function showen in fig.5., the lattice strain (ε) can be calculated if the value of Young's modulus of the nanoparticles is known, it is taken as 74.5 GPa for ZnS [12]. A summary of

these parameters (crystallite size, strain, stress and energy densities) calculated using UDM, UDSM, and UDEDM is presented in Table 1

Structural Parameters	UDM	UDSM	UDEDM	Scherrer
D (nm)	7.35	7.35	7.35	6.3
ε	0.0093	0.0093	0.0017	-------
σ(Pa) x 10^9	-----	7	1.2	-------
$\mu \times 10^5$ (J m^{-1})	-------	------	2.36	------
δ x10^{12} /m^2	1.8	1.8	1.8	2.5

Table (1): Micro-structural properties of ZnS nanoparticles

the UDEDM, UDM, and UDSM models confirmed a good agreement with the TEM analysis of the average crystallite size obtained with the results, so these models are acceptable in the present case. Also, The crystallites values presented from the three models are in good agreement with those obtained from Scherrer's formula and TEM.

3.2. Transmission electron microscopy measurements:

The typical morphology of the obtained ZnS nanoparticles was necessary to know thire exact size and structures by direct measurement as TEM. Fig.6 shows TEM images that sample shows the presence of large number of nearly spherical ZnS nanoparticles with distinct grain boundaries. The range particle size is found to be 8-10 nm, which is nearly consistent with the particle size obtained from XRD observations. Therefore, the diameter and the size distribution of the nanoparticles are difficult to be determined precisely by simply viewing the TEM image [11,13].
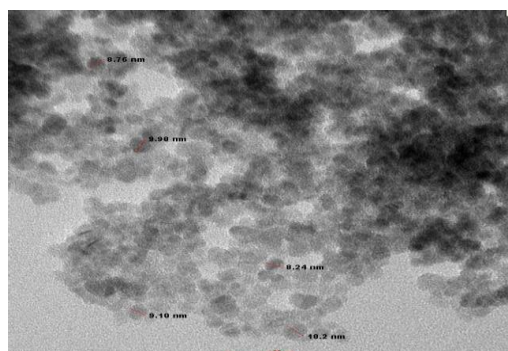
Fig. 6: TEM images of ZnS nanoparticles
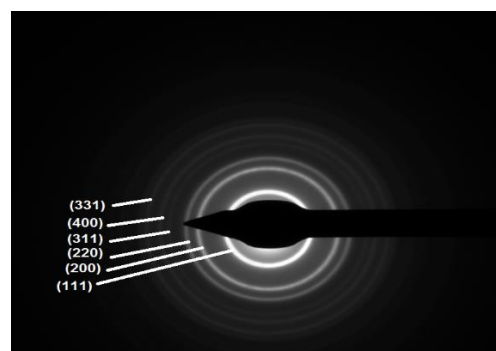
Fig.7: The SAED pattern of ZnS nanostructure.

Fig. 7 shows the Selected Area Electron Diffraction (SAED) pattern of ZnS nanoparticles. The SAED pattern shows a set of rings, which relate to diffraction from different planes of the ZnS nanocrystallites. The pattern shows many rings, among them the strongest six rings correspond to the (111), (200), (220), (311), (400), and (311) planes of the cubic phase of ZnS. This result is consistent with XRD analysis. It was observed that, the particles are well separated and in a spherical shape and it shows the present magnified view of nanocrystals.

3. 3 Thermal analysis measurement:

Fig. 8 represents a combined plot of TG and DTG to explore the stability and the transitions which might occur. TG curve of ZnS nanoparticles at a heating rate of 283 K min^{-1} under nitrogen atmosphere from room temperature up to 1100K. Due to strong water absorption of ZnS at 313K.
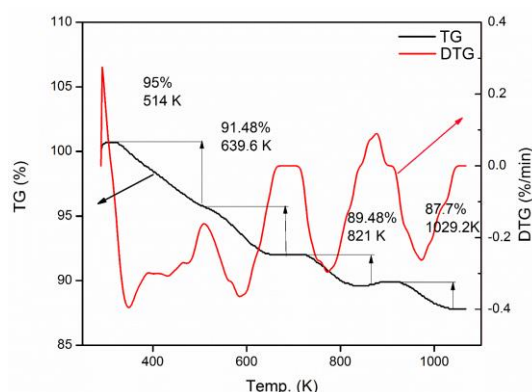
Fig. 8: TG and DTA thermograms of ZnS
nanopartic**les**
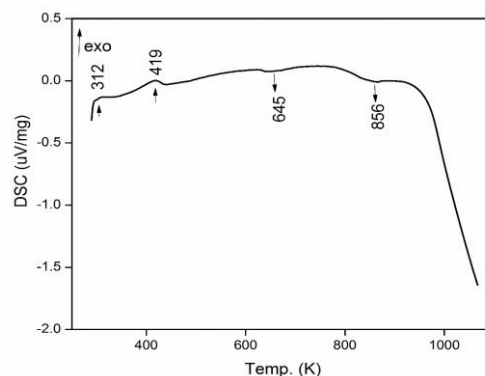
Fig. 9: FTIR spectra of ZnS nanoparticles

There are three obvious weight loss regions. The first weight loss is 5% and it is observed around 393K [14] due to some water molecules present in the Samples. The second stage of a weight loss starts at 639K, in which ZnS is converted into $ZnSO_3$ with weight loss of 2.2%, representing the evaporation and degradation of the sulphuric acid group [15]. Further mass loss has also been observed at 1029K, where $ZnSO_3$ is converted into ZnO with 2 % weight loss. Therefore, the total weight loss in ZnS is 9.2% from 323K to 1093K. It can be concluded that ZnS particles have good thermal stability.

Differential scanning calorimetry (DSC) measures endothermic and exothermic processes in materials as a function of temperature and heat flow The first exothermic peak was observed at 419K [16]. This peak was attributed to the evaporation of water molecules. The second strong endothermic peak was observed at 654K, probably corresponding to the lattice deformation of ZnS, but above 873 K in DSC curve, there was a smooth downward trend with significant weight loss. This may be due to the residual sulfur ions released from the sample.
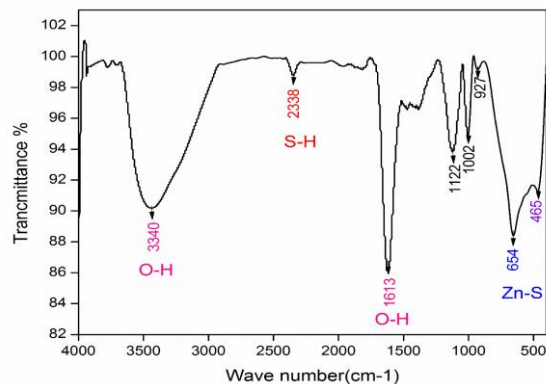
Figure 10. FTIR spectra of ZnS nanoparticles.

3.3. Infrared absorption spectra of ZnS nanoparticles

The infrared absorption spectra (FTIR) of ZnS recorded in the region from (400-4000) cm^{-1} is shown in Fig. 10. Spectrum analysis of ZnS shows that despite the successive washes powder with absolute ethanol traces of solvent still exist confirmed by the presence of a broad and intense band at around 3340 cm^{-1} assigned to the vibrations of the valence of O-H mode in H_2O molecules. This peak may be due to water present in a sample. The small and weak peak observed at 2338 cm^{-1} may be due to the formation of S-H bond (H_2S). The presence of a band around 1613 cm^{-1} [17] may be correspond to the O–H bending of water molecules [18], absorption at 1122 cm^{-1} was assigned to SO_4^{-}. The weak additional bands observed at 1002 cm^{-1} and 924 cm^{-1} [19] indicate the presence of resonance interaction between vibrational modes of sulfide ions in the crystal [19]. The vibration of the ZnS bond is confirmed by the presence of medium and strong bands located around 1122 and 654 cm^{-1} [20, 21] and the small and weak band at 465 cm^{-1} is assigned to the metal-sulfur bond.

3.4. A.C conductivity of ZnS nanocrystal:

The frequency dependence of AC conductivity in ZnS nanoparticles at different temperatures 293 -373 K. are shown in Fig. (11). The range of low frequency conductivity increases with temperature, while the temperature is independent in the high-frequency region. In addition, the conductivity is found to be frequency dependence less on the low-frequency regime.
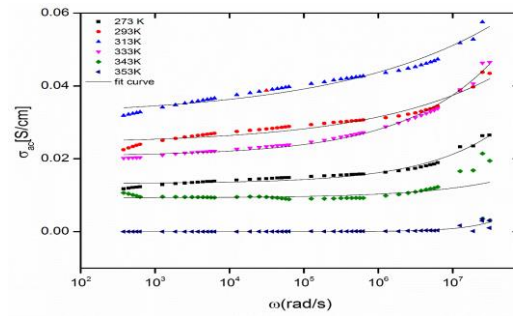
Figure 11. Frequency dependence of AC conductivity at various temperatures.
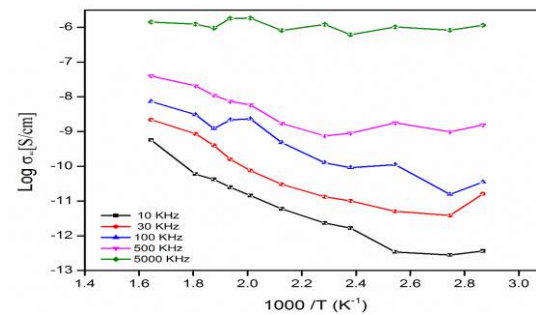
Figure 12. Temperature dependence of σ_{ac} (ω) for ZnS nanoparticles.

Fig.12 shows the variation of $\sigma_{ac}(\omega)$ versus 1000/T for studied composition at different frequency values. It is evident that A.C. conductivity decreases nonlinearly with the reciprocal of temperature, which suggests that σ_{ac} (ω) is a thermally, activated process with single activation energy from various localized states in the band gap. The activation energy of A.C. conduction has been calculated at different frequencies using the Arrhenius temperature dependence of σ_{ac} (ω) [22]. The activation energy ΔE_{ac} decreases with the frequency which may be attributed to the increasing field frequency which is responsible for the electronic jump between localized states [28]. The values of activation energy with the corresponding frequency are shown in the nearest table.

Frequency (Hz)	Activation Energy (eV)
10 K	0.22319
30 K	0.18
100 K	0.174
500 K	0.105
5 M	0.014

4. Conclusion

ZnS nanoparticles have been synthesized via low cost, easy, high yield precipitation method. Different techniques XRD and FTIR were used to achieve the formation of ZnS particles and XRD and TEM used to investigate the nanocrystal particles size and all in good agreement. Good thermal stability for the sensitized ZnS nanoparticles. The W–H deformation models (UDM, UDSM and UDEDM) were very helpful in determining the strain,

stress and energy density with a certain approximation, and hence these models are highly preferable to define the crystal perfection. The temperature and frequency dependence of A.C conductivity $\sigma_{ac}(\omega)$ are studied in the frequency range 50 Hz-5×10^6 Hz and temperature range 293 -373 K.

References

1. Soltani N., Saion E., Hussein M. Z., Erfani M., Abedini A., Bahmanrokh G., Navasery M. & Vaziri P., 2012, Visible Light-Induced Degradation of Methylene Blue in the Presence of Photocatalytic ZnS and CdS Nanoparticles. Int. J. Mol. Sci. 13, 12242–12258.

2. Al-Rasoul K. T., Ibrahim I. M., Ali I. M. & Al-Haddad R. M. 2014, Synthesis, structure and characterization of ZnS QDs and using it in photocatalytic reaction. Int. J. Sci. Technol. Res. 3, 213–217.

3. Hoa T. T. Q., Vu L. V., Canh T. D. & Long N. N. Journal of Physics: Conference Series, 2009, 187, 01-06

4. Liveri V.T., Rossi M., D'Arrigo G., Manno D., Micocci G. A 1999, Synthesis and characterization of ZnS nanoparticles in water/AOT/n-heptane microemulsions. Appl. Phys., 69, 369–373.

5. Soltani N., Dehzangi A., Kharazmi A., Saion, E., Yunus W. M. M., Majlis B. Y., Zare M. R., Gharibshahi E. & Khalilzadeh N. 2014, structural optical and electrical properties of zns nanoparticles affecting by organic coating . Chalcogenide Letters, 11(2), 79 - 90.

6. Simbrunner J. , Simbrunner C. , Schrode B. , Röthel C. , Martinez N. B., Salzmann I. & Resel R., 2018, Indexing of grazing-incidence X-ray diffraction patterns: the case of fibre-textured thin films. Acta Cryst. A74, 373-387

7. Date E. H. F. & Andrews K. W., 1969, Anisotropic and composition effects in the elastic properties of polycrystalline metals. Journal of Physics D: Applied Physics, 2(10), 13-21.

8. Rogers K., & Daniels P., Biomaterials, 2002, An X-ray diffraction study of the effects of heat treatment on bone mineral microstructure. 23(12), 2577-2585.

9. Chandrasekar L. B., Chandramohan R., Vijayalakshmi R., Chandrasekaran S., 2015, Preparation and characterization of Mn-doped ZnS nanoparticles. Nano Letters. 5(2), 71-5.

10. Thandavan T. M. K., Gani S. M. A., Wong C. S. & Nor R. M., 2015, Evaluation of Williamson–Hall Strain and Stress Distribution in ZnO Nanowires Prepared Using Aliphatic Alcohol. Journal of Nondestructive Evaluation, 34(2), 4-14.

11. Mochahari K. & Sarma K. C., 2013, Study of structural and optical properties of chemically synthesized nanostructured cadmium zinc sulphide films for band gap tunability. Scientific Engineering and Technology Research, 2(18), 2067-70.

12. Raleaooa P. V., Roodt A., Mhlongo G. G., Motaung D. E., & Ntwaeaborwa M. O., 2018, Analysis of the structure, particle morphology and photoluminescent properties of ZnS:Mn2+ nanoparticulate phosphors. Optik, 153, 31-42.

13. Ayodhya D., Venkatesham M., Kumari A. S., Mangatayaru K. G. & Veerabhadram G., 2013, Synthesis, Characterization of ZnS nanoparticles by

14. Coprecipitation method using various capping agents Photocatalytic activity and Kinetic study. IOSR Journal of Applied Chemistry, 6, 01-09

15. Chandrakanthi N., & Careem M. A., 2000, Thermal stability of polyaniline. Polymer Bulletin, 44, 101-108.

16. Sharma A. L., Saxena V., Annapoorni S. & Malhotra B. D., 2001, Synthesis and characterization of a copolymer: Poly(aniline-co-fluoroaniline). Journal of Applied Polymer Science, 81, 1460–1466.

17. Suganthi N. & Pushpanathan K., 2018, Photocatalytic degradation and ferromagnetism in mesoporous La doped ZnS nanoparticles. Materials Science: Materials in Electronics, 29(16), 13970-13983.

18. Viswanath R., Naik, H. S. B., Somalanaik Y. K. G., Neelanjeneallu P. K. P., Harish K. N., & Prabhakara, M. C., 2014, Studies on Characterization, Optical Absorption, and Photoluminescence of Yttrium Doped ZnS Nanoparticles. Journal of Nanotechnology, 2014, 1-8.

19. Mailhot B., Morlat S. & Gardette J. L., 2000, Photooxidation of blends of polystyrene and poly(vinyl methyl ether): FTIR and AFM studies. Polymer, 41(6), 1981-1988.

20. Prasad B. E., Kamath P. V., & Upadhya S., 2008, Electrochemical Synthesis of Macroporous Oxide Coatings on Stainless-Steel Substrates. the American Ceramic Society, 91(12), 3870–3874

21. 20. Ezzaier H., Guegan R., Muller F., Amara B. H. M. & Ben Rhaiem H., 2014,Dielectric properties of ZnS filled polystyrene nanoparticules. Innovation and Applied Studies, 9, 29-36

22. Zhao Y., Wang F., Fu Q., & Shi, W., Polymer, 2007, Synthesis and characterization of ZnS/hyperbranched polyester nanocomposite and its optical properties. 48(10), 2853-2859.

23. Raj F. M., Sathish R. & Rajendran A. J., (2016), Scientific Research and Modern Education , 4(7), 69-77.